



Discovery of potent, selective and orally bioavailable imidazo[1,5-*a*]pyrazine derived ACK1 inhibitors

Meizhong Jin*, Jing Wang, Andrew Kleinberg, Mridula Kadalbajoo, Kam W. Siu, Andrew Cooke, Mark A. Bittner, Yan Yao, April Thelemann, Qunsheng Ji, Shripad Bhagwat, Kristen M. Mulvihill, Josef A. Rechka, Jonathan A. Pachter, Andrew P. Crew, David Epstein, Mark J. Mulvihill

OSI Pharmaceuticals, LLC, A Wholly-Owned Subsidiary of Astellas US LLC, 1 Bioscience Park Drive, Farmingdale, NY 11735, USA

ARTICLE INFO

Article history:

Received 27 October 2012

Revised 12 December 2012

Accepted 13 December 2012

Available online 21 December 2012

Keywords:

Activated Cdc42-associated kinase (ACK1)

Inhibitors

Structure–activity relationships (SAR)

Imidazo[1,5-*a*]pyrazine

Cancer

ABSTRACT

This Letter describes the medicinal chemistry effort towards a series of novel imidazo[1,5-*a*]pyrazine derived inhibitors of ACK1. Virtual screening led to the discovery of the initial hit, and subsequent exploration of structure–activity relationships and optimization of drug metabolism and pharmacokinetic properties led to the identification of potent, selective and orally bioavailable ACK1 inhibitors.

© 2012 Elsevier Ltd. All rights reserved.

Activated Cdc42-associated kinase (ACK1) is a non-receptor tyrosine kinase originally identified by virtue of its binding to GTP-bound small GTPase Cdc42.¹ It is ubiquitously expressed and is activated by multiple extracellular growth factors such as EGF, PDGF, and TGFβ. Upon activation, ACK1 mediates a signaling cascade by directly interacting with and phosphorylating downstream effectors.² Considerable attention has been paid to the biological function of ACK1 in recent years especially to its involvement in cancer.³ For example, gene amplification and over-expression of ACK1 were found in multiple cancers including lung, ovarian and prostate cancers and were associated with poor prognosis and metastatic phenotypes.⁴ Activated ACK1 has been shown to phosphorylate and activate androgen receptor function and to promote the progression of prostate cancer.⁵ More recently, activated ACK1 was found to phosphorylate and promote the activation of Akt, a protein kinase that plays a central role in growth, proliferation and cell survival in various cancers.⁶ Taken together, these literature data suggest that ACK1 is a potential target for cancer treatment. Moreover, a potent and selective small molecule ACK1 inhibitor will provide a valuable tool to help to further probe the role of ACK1 in cancer.

A series of pyrazolo[3,4-*d*]pyrimidines has been previously disclosed as ACK1 inhibitors.⁷ Compound **1** is a representative

example from this series with a reported ACK1 cellular mechanistic IC₅₀ value of 20 nM (Fig. 1). A series of 5,6-biaryl-furo[2,3-*d*]pyrimidines and bioisosteric 2,3-diaryl-furo[2,3-*b*]pyridines and 5,6-biaryl-pyrrolo[2,3-*d*]pyrimidines have also been reported as potent ACK1 inhibitors.⁸ For example, compound **2a** inhibits ACK1 in a cellular mechanistic assay with an IC₅₀ value of 10 nM. Another compound from this class, AIM-100 (compound **2b**, Fig. 1) moderately inhibits ACK1 with a cellular mechanistic IC₅₀ value of 0.62 μM, suppressing both ACK1 Tyr284- and androgen receptor Tyr267-phosphorylations in vitro.^{8d,9} Unfortunately, these disclosed compounds suffered poor oral pharmacokinetic (PK) properties due to metabolic instability which prevented them from being utilized further in the in vivo setting. Herein we report our drug discovery effort around small molecule ATP competitive ACK1 inhibitors. More specifically, the initial discovery, optimization and in vitro and in vivo characterization of a series of imidazo[1,5-*a*]pyrazine-derived inhibitors of ACK1 which possessed favorable drug-like properties including potency, selectivity and orally bioavailability.

Our initial approach to identify hits was two-pronged and included a high-throughput screening (HTS) campaign of the OSI compound library as well as a virtual screening (VS) campaign, utilizing a publically available crystal structure of ACK1 (PDB code: 1U4D). A tolerance for protein flexibility was incorporated into the virtual screening design with the hope of identifying hits which would require diverse protein conformations for binding, since such potential hits might be rejected if a rigid protein structure

* Corresponding author.

E-mail address: Meizhong.jin@astellas.com (M. Jin).

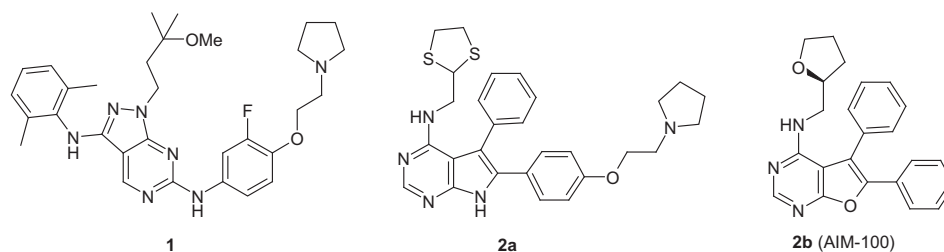


Figure 1. Representative ACK1 inhibitors disclosed in literature.

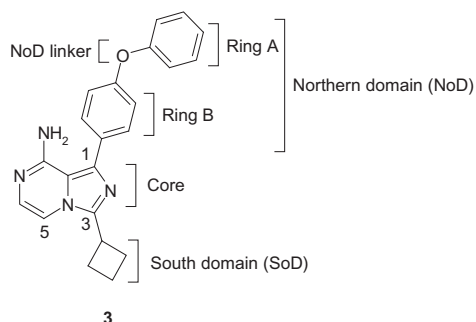


Figure 2. Imidazo[1,5-*a*]pyrazine hit, compound **3**, discovered from ACK1 virtual screening.

was used. In order to confirm the potency of prioritized virtual screening hits, an Alpha-screen assay (ATP concentration of 100 μM)¹⁰ was implemented where the low molecular weight (MW = 356) imidazo[1,5-*a*]pyrazine-derived compound **3** (Fig. 2) emerged as a potent hit ($\text{IC}_{50} = 0.19 \mu\text{M}$). Detailed computational studies were then performed on compound **3**, with some of the major modeled interactions between this compound and ACK1 highlighted in Figure 3. The C8-amino group and N7 of the imidazo[1,5-*a*]pyrazine core of the compound form two hydrogen bonds with the hinge backbone amides. The 4-phenoxyphenyl moiety, termed the northern domain (NoD), substituted from the C1 position of the core, passes through a channel occupied by gatekeeper Thr205, with the ring A moiety further extending into a lipophilic pocket primarily formed by Val178 and Met181 of the αC -helix as well as Leu192, Met203, Thr205 and Phe271 (F of the DFG loop). Furthermore, modeling studies suggested a protein conformational change associated with this proposed binding mode, since the accommodation of ring A of **3** required an enlargement of the back pocket from its original size which was not evident

from the initial static view of the crystal structure (PDB code: 1U4D). The cyclobutyl moiety, termed the southern domain (SoD), emanating from C3 of the core, extends past the glycine rich P-loop and towards the solvent exposed region of the protein.

To further explore and build SAR around compound **3**, we first sought to analog around the NoD moiety and specifically ring A while keeping the rest of the molecule constant (Table 1). Various substitutions encompassing different sizes and electronic properties were walked around the ring. While C2-F (compound **4**) and C3-F (compound **7**) substitutions offered a slight increase in potency, all other substitutions resulted in a loss of potency. In the C4 position of ring A, substitution consistently resulted in a loss of potency. This observation was in agreement with modeling predictions which suggested that phenyl as ring A optimally fit into this hydrophobic pocket as there is not enough additional space available to accommodate further substituents. Pyridyl variant **13** was also evaluated and found to be inferior to the phenyl group in terms of ACK1 potency, most likely due to an unfavorable desolvation penalty introduced by the pyridine nitrogen atom. Replacement of ring A with alkyl groups such as methyl, isopropyl and cyclohexyl groups abolished potency (data not shown), suggesting phenyl is an optimal pharmacophoric element at this position.

We next sought to explore the SAR around the proximal phenyl ring (ring B) of the NoD moiety. While using phenyl as a template for ring B, modeling studies suggested that a hydrogen bond acceptor substituted off the C2' position could form a hydrogen bond interaction with the side chain hydroxyl group of the gatekeeper Thr205 and thus may improve potency. As shown in Table 2, while both C2'-OMe (compound **14**, Fig. 4a) and C2'-F (compound **15**) substitutions increased potency over **3**, C2'-Cl (compound **16**) and C2'-Me (compound **17**) substitutions decreased potency. These results, when taken together, helped to further validate the model. Other hydrogen bond acceptor moieties evaluated at this position such as amides (compounds **18–19**) generally abolished potency

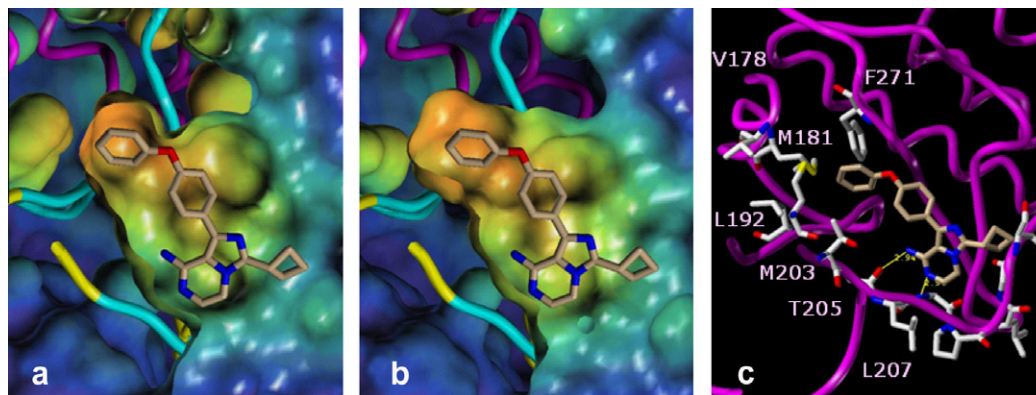
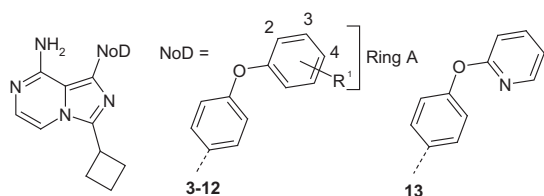
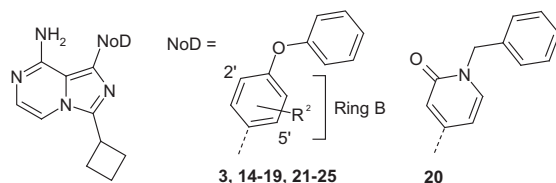


Figure 3. Modeled interactions of compound **3** with ACK1. (a) Section view of ACK1 surface based on the initial crystal structure (PDB code: 1U4D) after removing the original ligand and manually placing compound **3** without energy minimization. (b) Section view of ACK1 surface after energy minimization of the complex with compound **3** where the enlargement of the back pocket is evident. (c) Critical interactions in the minimized modeling structure.

Table 1
SAR of NoD moiety–ring A

Compd	R ¹	ACK1 biochem IC ₅₀ ^a (μM)
3	H	0.19
4	2-F	0.10
5	2-Me	0.24
6	2-Cl	0.74
7	3-F	0.11
8	3-Me	0.24
9	3-Cl	3.19
10	4-F	5.46
11	4-Me	0.90
12	4-Cl	1.87
13		1.90

^a Throughout this Letter, all IC₅₀ values are an average of at least two values.

Table 2
SAR of NoD moiety–ring B

Compd	R ²	ACK1 biochem IC ₅₀ (μM)
3	H	0.19
14	2'-OMe	0.048
15	2'-F	0.088
16	2'-Cl	1.69
17	2'-Me	6.28
18	2'-NHCOMe	>10
19	2'-CONH ₂	>10
20		>10
21	5'-F	0.22
22	5'-Me	0.37
23	5'-Cl	1.06
24	5'-OMe	0.075
25	5'-OEt	0.47

Table 3
Quantum chemistry calculation of the total energy $\Delta\Delta E^a$ of compounds **14** and **20** with respect to **3**

Compd	$\Delta\Delta G_s^b$	$\Delta\Delta E_c^c$	$\Delta\Delta E_i^d$	$\Delta\Delta E$	ACK1 biochem IC ₅₀ (μM)
3	0	0	0	0	0.19
14	0.38	0.78	-3.72	-2.56	0.048
20	9.13	2.53	-5.62	6.04	>10

^a $\Delta\Delta E = \Delta\Delta G_s + \Delta\Delta E_c + \Delta\Delta E_i$.

^b $\Delta\Delta G_s$: The difference of the solvation free energies of compounds **14** and **20** compared to that of compound **3**.

^c $\Delta\Delta E_c$: The difference of energy cost associated with conformational changes of compounds **14** and **20** before and after binding compared to that of compound **3**.

^d $\Delta\Delta E_i$: The difference of interaction energies of compounds **14** and **20** compared to that of compound **3**.

as this was most likely caused by steric clashes with the protein due to limited binding space in this region. Interestingly, pyridone analog **20** was found to be inactive although there were no steric issues in binding as suggested by modeling, and the pyridone carbonyl is a strong hydrogen bond acceptor based on its pK_{BHX} value.¹¹ To further clarify this apparent discrepancy, we performed quantum chemistry calculations on binding interactions of compounds **3**, **14** and **20**.¹² As shown in Table 3, compound **20** indeed formed a stronger hydrogen bond interaction with Thr205 compared to **14** as indicated by a more favorable interaction energy gain ($\Delta\Delta E_i$) but suffered a much greater energy loss due to an increased desolvation penalty ($\Delta\Delta G_s$) and adverse conformational changes ($\Delta\Delta E_c$). As a result, compound **20** had an overall energetically unfavorable interaction ($\Delta\Delta E$) which rendered it inactive.

In terms of the ring B C5' position, while C5'-F (compound **21**) was tolerated, C5'-Me (compound **22**) and C5'-Cl (compound **23**) substitutions resulted in a loss in potency. However, the C5'-OMe substitution (compound **24**) resulted in a ~3-fold increase in potency compared to **3**. Modeling suggested a pseudo hydrogen bond interaction between the C5'-OMe group and the carbonyl of Gly269 (Table 3, Fig. 4b).¹³ A C5'-OEt substitution (compound **25**) resulted in a decrease in potency, speculated to be due to the bulkier ethoxy group and the ensuing desolvation of Asn257, Arg256 and Gly269.

The SAR around the NoD linker moiety which connects rings A and B was also explored (Table 4). This effort primarily focused on one-atom-length tethers, due to the concern that an extended linker would simply push ring A into a steric clash with the protein, as suggested by modeling and SAR previously established and highlighted in Table 1. Various bioisosteric replacements to the oxygen linker in compound **3** were generally tolerated with the observation of less than threefold loss of potency (compounds

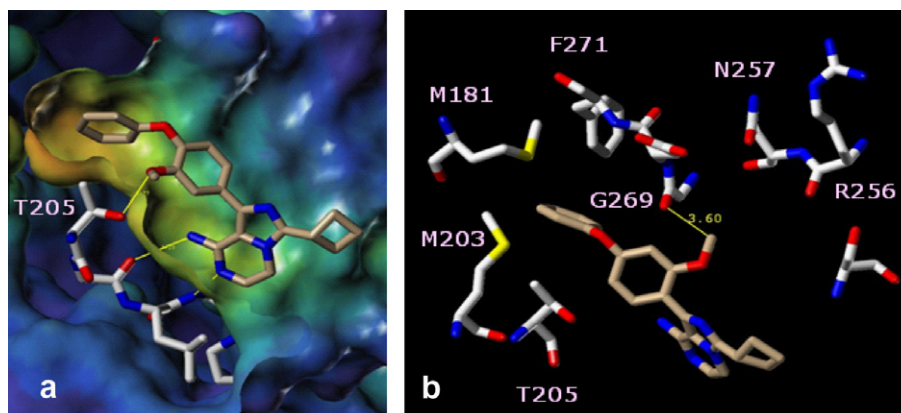
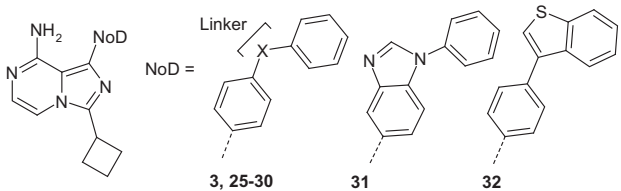


Figure 4. Modeled interactions of compounds **14** and **24** with ACK1. (a). The C2'-OMe group of **14** forms a hydrogen bond with Thr205 (MeO...OH distance: 2.77 Å); (b) the C5'-OMe group of **24** forms a pseudo hydrogen bond with Gly269 carbonyl (C(H₂)-H...O=C distance: 3.60 Å).

Table 4
SAR of NoD linker moiety



Compd	X	ACK1 biochem IC ₅₀ (μM)
3	O	0.19
25	S	0.33
26	NH	0.38
27	CH ₂	0.57
28	C=O	0.087
29	CHOH	0.28
30	C(OH)Me	0.090
31		3.35
32		4.09

25–27). Several variants of the carbon based linker such as carbonyl (compound **28**) and alcohols (compound **29**, **30**) showed increased potency over compound **27**. This was rationalized through the model where these linkers formed hydrogen bond

interactions with Lys158. Several 5,6-cyclized systems (compounds **31**, **32**) suffered significant losses of potency, speculated to be due to the inability to adopt the required bioactive conformation possessed by **3** (Fig. 3). Subsequently, we successfully obtained a co-crystal structure of compound **33**, a close analog of **3**, with the ACK1 kinase domain (PDB code: 4ID7). The interactions revealed in this co-crystal structure essentially confirmed the binding mode proposed by modeling, including the predicted enlargement of the back pocket to accommodate ring A of the NoD moiety (Fig. 5).

While expanding the SAR around the NoD moiety, we conducted a mouse PK study on compound **3** to benchmark its DMPK properties. As summarized in Table 5, at an oral dose of 20 mg/kg, compound **3** displayed good oral bioavailability (50%) with a moderate exposure as indicated by a plasma C_{max} of 0.9 μM. The intravenous clearance was higher than mouse liver blood flow (~90 mL/min/kg), as was predicted by the high mouse hepatic extraction ratio (mouse ER = 0.89) observed upon in vitro incubation in microsomes. Furthermore, two significant M + 16 metabolites were detected in both oral (~65% of parent AUC) and intravenous plasma samples (~20% of parent AUC). Mass fragmentation analysis suggested that both metabolites were produced from hydroxylation of the cyclobutyl southern domain moiety (SoD) via a phase-I mechanism. Compound **33** was synthesized and confirmed as one of the metabolites based on LC–MS/MS (the other

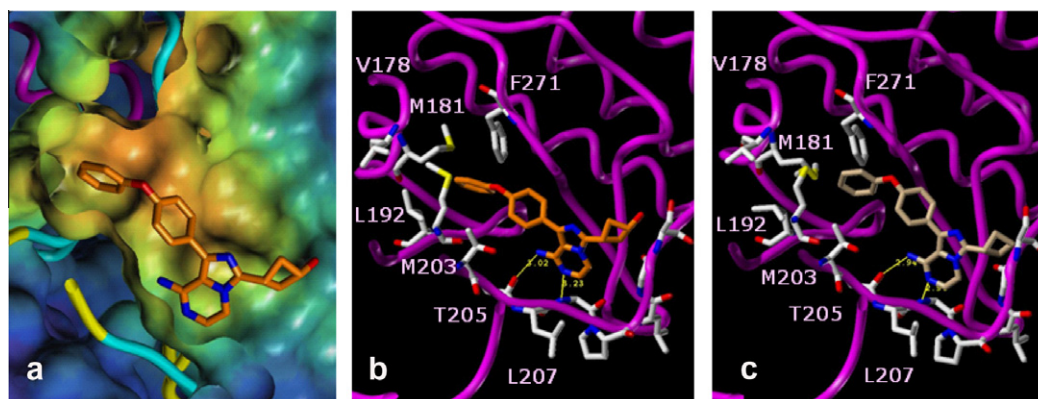
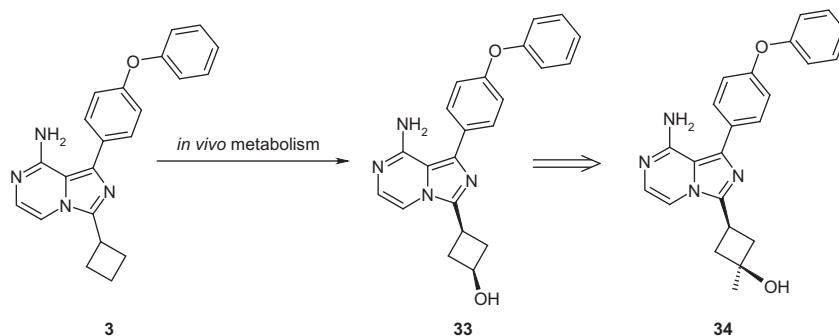


Figure 5. Co-crystal structure of ACK1 and **33** (PDB code: 4ID7) along with a side-by-side comparison with the predicted modeling structure. (a) Section view of ACK1 surface in complex with **33** based on the co-crystal structure. (b) Critical interactions between **33** and ACK1 in the co-crystal structure. (c) Critical interactions between **3** and ACK1 in the modeling structure.

Table 5
Key mouse PK parameters of compounds **3**, **34**



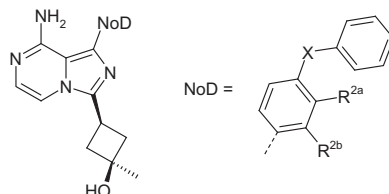
Compd	Mouse oral PK (20 mg/kg)				Mouse iv PK (2 mg/kg)	
	C _{max} (μM)	AUC (ng h/mL)	t _{1/2} (h)	F%	V _{ss} (L/kg)	CL (mL/min/kg)
3	0.9	1236	5.5	50	9.0	135
34	11.2	4680	4.9	87	1.7	62

metabolite was speculated to be the *trans*-isomer). Compound **34** was subsequently synthesized where the C3 position of cyclobutyl moiety was fully substituted in order to block this primary route of metabolism. To our satisfaction, compound **34** maintained similar

potency (biochem IC₅₀ = 0.16 μM) to that of compound **3** while showing significantly improved in vitro microsomal stability (mouse ER = 0.60). A mouse PK study with compound **34** showed significantly improved oral exposure, decreased intravenous

Table 6

Combination of preferred SoD and NoD pharmacophores



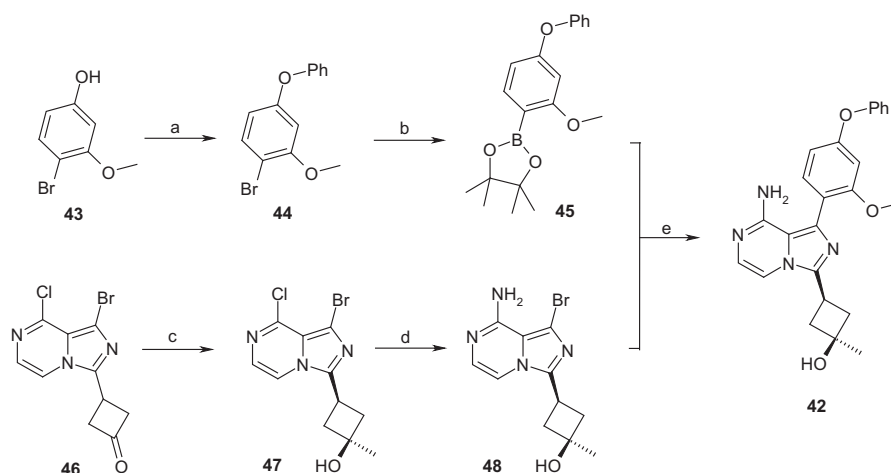
Compd	R ^{2a}	R ^{2b}	X	ACK1 biochem IC ₅₀ (μM)	ACK1 cell mech. IC ₅₀ (μM)	E.R. (m/h)
35	F	H	C=O	0.14	0.030	0.71/0.93
36	OMe	H	C=O	0.11	0.029	0.50/0.91
37	H	F	C=O	0.088	0.028	0.86/0.86
38	H	H	CH ₂	0.23	0.058	0.77/0.81
39	H	H	CF ₂	0.45	0.17	0.65/0.63
40	H	H	C(OH)Me	0.22	0.084	0.52/0.57
41	F	F	O	0.13	0.051	0.53/0.77
42	H	OMe	O	0.11	0.035	0.55/0.53

Table 7Key mouse PK parameters of compounds **39**, **40** and **42**

Compd	Mouse oral PK (20 mg/kg)				Mouse iv PK (2 mg/kg)	
	C _{max} (μM)	AUC (ng h/mL)	t _{1/2} (h)	F%	V _{ss} (L/kg)	CL (mL/min/kg)
39	5.0	8544	4.3	160	1.7	63
40	4.6	3943	2.6	105	3.3	89
42	5.9	8484	3.8	98	1.8	39

Table 8Physicochemical and ADMET properties of compound **42**

CYP inhibition	IC ₅₀ (μM)	Miscellaneous physicochemical and ADMET properties
CYP1A2	>20	MW/A log P/PSA
CYP2C9	>20	PAMPA (10 ⁻⁶ cm/s)
CYP2C19	16.3	
CYP2D6	>20	Aq solubility
CYP3A4	>20	hERG (IC ₅₀)
		416/3.16/94.9 (Å)
		591 (pH 7.4)
		280 (pH 5.0)
		>100 μM (pH 7.4)
		>15 μM



Scheme 1. Reagents and conditions: (a) PhB(OH)₂, Cu(OAc)₂, Et₃N, DCM, rt, 42%; (b) PdCl₂(dppf), KOAc, bis(pinacolato)diboron, dioxane, 80 °C, 75%; (c) MeMgCl, THF, −78 °C, 70%; (d) NH₃ in water (35%), 2-butanol, 90 °C, 95%; (e) PdCl₂(dppf), K₂CO₃, dioxane–water (4:1, v:v), 95 °C, 68%.

clearance with no significant metabolites detected in plasma. Subsequently, a systematic SAR exploration around the SoD (data not shown) revealed that the methyl cyclobutanol moiety shown in compound **34** was a preferred pharmacophoric element for this region of the molecule.

After extensive SAR exploration on key pharmacophoric elements as described above, preferred SoD and NoD groups were merged, with a representative list of compounds highlighted in Table 6. Compounds with carbonyl and methylene NoD linkers (**35–38**) gave both good biochemical and cellular mechanistic potencies¹⁴ but less optimal DMPK properties as indicated by relatively high extraction ratios (low microsomal stability) in both mouse and human liver microsomes. Compound **39**, with a gem-difluoromethylene linker, showed improved microsomal stability, however, it suffered a moderate potency loss. Compound **40** with the tertiary alcohol linker motif and compounds **41–42** with an oxygen linker demonstrated both good potency and good microsomal stability. Key compounds were progressed to mouse PK studies and the results are summarized in Table 7. All three compounds tested had good oral exposures and were highly bioavailable with moderate rates of clearance. It should be noted that in these studies, compound **40** was evaluated as a racemic mixture. The enantiomers were later separated by chiral supercritical fluid chromatography (SFC) and subjected to mouse PK studies. Both enantiomers showed similar PK profiles to **40**, with no racemization detected in vivo by chiral HPLC analysis of the plasma samples.

To understand the kinase selectivity profile of this series, compound **42**, as a representative analog from this series, was profiled against 216 purified protein kinases representing the tyrosine and serine/threonine kinase families using an in-house Caliper EZ Reader mobility shift assay. Assays were conducted with the concentration of ATP at K_m for each individual kinase with compound **42** at a concentration of 1.0 μM . Among 216 kinases screened, compound **42** showed ~100% inhibition of ACK1 and >80% inhibition of 12 other kinases. Of the 12 off-target kinases, none were considered major cell growth drivers such as receptor tyrosine kinases or cell-cycle regulating kinases.¹⁵ The selectivity was further confirmed by KINOMscan profiling against an even larger panel of 451 kinases, where compound **42** showed a selectivity score of $S(10) = 0.08$, which represents a relatively high degree of selectivity.¹⁶ Compound **42** possesses favorable drug-like properties as indicated by its physicochemical and ADMET properties, as summarized in Table 8. A convergent synthesis of compound **42** is illustrated in Scheme 1. Phenol **43** was converted to di-phenyl ether **44** though a Cu(II) mediated Chan–Lam coupling,¹⁷ the subsequent palladium catalyzed borylation of **44** afforded the desired boronate **45**. The key imidazo[1,5-*a*]pyrazine intermediate **46** was treated with methyl Grignard reagent MeMgCl followed by an ammonolysis to give compound **48**, which then underwent a Suzuki coupling with boronate **45** to provide compound **42**.¹⁰

In summary, a series of imidazo[1,5-*a*]pyrazine derived ACK1 inhibitors was identified through a combination of structure-based drug design and empirical medicinal chemistry efforts. Efforts originated from virtual screening hit **3**, where SAR exploration and DMPK optimizations eventually led to compound **42**, a potent and selective ACK1 inhibitor with favorable in vitro physicochemical and ADMET properties. Furthermore, compound **42**

demonstrated good in vivo PK properties, which makes it a valuable compound to probe the in vivo biology of ACK1.

Acknowledgments

The authors gratefully acknowledge Dr. Yingjie Li and Ms. Viorica M. Lazarescu for analytical support; Mr. Paul Maresca, Mr. Pete Meyn and the Leads Discovery Group for conducting in vitro AD-MET studies; The authors also gratefully acknowledge Proteros Biostructures GmbH for collaboration on ACK1 co-crystallization effort.

References and notes

- Manser, E.; Leung, T.; Salihuddin, H.; Tan, L.; Lim, L. *Nature* **1993**, *27*, 364.
- Prieto-Echague, V.; Miller, W. T. *J. Signal Transduct.* **2011**, article ID 742372.
- (a) Mahajan, K.; Mahajan, N. P. *J. Cell. Physiol.* **2010**, *224*, 327; (b) Chua, B. T.; Lim, S. J.; Tham, S. C.; Poh, W. J.; Ullrich, A. *Mol. Oncol.* **2010**, *4*, 323.
- Van der Horst, E. H.; Degenhardt, Y. Y.; Strelow, A.; Slavina, A.; Chinn, L.; Orf, J.; Rong, M.; Li, S.; See, L. H.; Nguyen, K. Q.; Hoey, T.; Wesche, H.; Powers, S. *Proc. Natl. Acad. Sci. U.S.A.* **2005**, *102*, 15901.
- (a) Mahajan, N. P.; Whang, Y. E.; Mohler, J. L.; Earp, H. E. *Cancer Res.* **2005**, *65*, 10514; (b) Mahajan, N. P.; Liu, Y.; Majumder, S.; Warren, M. R.; Parker, C. E.; Mohler, J. L.; Earp, H. S.; Whang, Y. E. *Proc. Natl. Acad. Sci. U.S.A.* **2007**, *104*, 8438.
- Mahajan, K.; Coppola, D.; Challa, S.; Fang, B.; Chen, Y. A.; Zhu, W.; Lopez, A. S.; Koomen, J.; Engelman, R. W.; Rivera, C.; Muraoka-Cook, R. S.; Cheng, J. Q.; Schönbrunn, E.; Sebt, S. M.; Earp, H. S.; Mahajan, N. P. *PLoS One* **2010**, *5*, e9646.
- Kopecky, D.; Hao, X.; Chen, Y.; Fu, J.; Jiao, X.; Jaen, J.; Cardozo, M.; Liu, J.; Wang, Z.; Walker, N.; Wesche, H.; Li, S.; Farrelly, E.; Xiao, S.; Kayser, F. *Bioorg. Med. Chem. Lett.* **2008**, *18*, 6352.
- (a) Kopecky, D.; Burkitt, S.; Clase, A.; Farelli, E.; Farthing, C.; Faulder, P.; Frenkel, D.; Harrison, M.; Jaen, J.; Jiao, X.; Kayser, F.; Li, S.; Liu, J.; Lively, S.; Sharma, R.; Strelow, A.; Van der Horst, E.; Wang, Z.; Wesche, H.; Xiao, S. *Abstracts of Papers, 232nd National Meeting of the American Chemical Society, San Francisco, CA; American Chemical Society: Washington, DC, 2006, MEDI 106*; (b) Liu, J.; Sharma, R.; Lively, S.; Burkitt, S.; Clase, A.; Farthing, C.; Jiao, X. Y.; Kopecky, D.; Kayser, F.; Shuttelworth, S.; Harrison, M.; Faulder, P.; Li, S.; Wesche, H.; Mallari, R.; Farrelly, E.; Xiao, S. -H.; Liu, J.; Wang, Z.; Jaen, J. *Abstracts of Papers, 232nd National Meeting of the American Chemical Society, San Francisco, CA; American Chemical Society: Washington, DC, 2006, MEDI 105*; (c) Lively, S.; Burkitt, S.; Cardozo, M.; Clase, A.; Farelli, E.; Farthing, C.; Faulder, P.; Harrison, M.; Jaen, J.; Jiao, X.; Kayser, F.; Kopecky, D.; Li, S.; Liu, J.; Liu, J.; Mallari, R.; Sharma, R.; Strelow, A.; Van der Horst, E.; Wang, Z.; Wesche, H.; Xiao, S. *Abstracts of Papers, 232nd National Meeting of the American Chemical Society, San Francisco, CA; American Chemical Society: Washington, DC, 2006, MEDI 107*; (d) Jiao, X.; Kopecky, D. J.; Liu, J.; Liu, J.; Jaen, J. C.; Cardozo, M. G.; Sharma, R.; Walker, N.; Wesche, H.; Li, S.; Farrelly, E.; Xiao, S. H.; Wang, Z.; Kayser, F. *Bioorg. Med. Chem. Lett.* **2012**, *22*, 6212.
- Mahajan, K.; Challa, S.; Coppola, D.; Lawrence, H.; Luo, Y.; Gevariya, H.; Zhu, W.; Chen, Y.; Lawrence, N.; Mahajan, N. P. *Prostate* **2010**, *70*, 1274.
- Crew, A. P.; Jin, M.; Kadalbajoo, M.; Kleinberg, A.; Mulvihill, M. J.; Wang, J. US 20090286768. Detailed biochemical assay and cellular mechanistic assay protocols, as well as synthesis of key intermediates and final compounds are described therein.
- Laurence, C.; Brameld, K. A.; Graton, J.; Le Questel, J. Y.; Renault, E. *J. Med. Chem.* **2009**, *52*, 4073.
- The calculations were performed with Jaguar program version 6.5 licensed from Schrodinger, Inc., Poland, OR. The B3LYP functional and 6-31G** basis set were used. To obtain the free state conformation of a compound, the geometrical optimizations with multiple starting points were performed.
- Bissantz, C.; Kuhn, B.; Stahl, M. *J. Med. Chem.* **2010**, *53*, 5061.
- The ACK1 biochemical potencies and cellular mechanistic potencies for this series of compounds are well correlated ($R^2 = 0.76$).
- Compound **42** showed >80% inhibition to following kinases (other than ACK1) when screened at 1.0 μM against 216 kinases: BLK, FGR, FRK, FYN, HCK, LCK, LYNB, SRC, SRMS, TEC, TXK, YES.
- Selectivity score is a quantitative measure of compound selectivity. It is calculated as such: selectivity score = (number of hits)/(number of assays). $S(10)$ is calculated using 10% control as a potency threshold: $S(10) = (\text{number of kinases with \% control} < 10) / (\text{number of kinases tested})$. Further information regarding to selectivity score is available at <http://www.kinomescan.com>.
- Evans, D. A.; Katz, J. L.; West, T. R. *Tetrahedron Lett.* **1998**, *39*, 2937.